

# PWC-Net: CNNs for Optical Flow Using Pyramid, Warping, and Cost Volume

Deqing Sun, Xiaodong Yang, Ming-Yu Liu, and Jan Kautz  
NVIDIA

## Abstract

We present a compact but effective CNN model for optical flow, called PWC-Net. PWC-Net has been designed according to simple and well-established principles: pyramidal processing, warping, and the use of a cost volume. Cast in a learnable feature pyramid, PWC-Net uses the current optical flow estimate to warp the CNN features of the second image. It then uses the warped features and features of the first image to construct the cost volume, which is processed by a CNN to estimate the optical flow. PWC-Net is 17 times smaller in size and easier to train than the recent FlowNet2 model. Moreover, it outperforms all published methods on the MPI Sintel final pass and KITTI 2015 benchmarks, running at about 35 fps on Sintel resolution ( $1024 \times 436$ ) images. Our model will be publicly available.

## 1. Introduction

Optical flow estimation is a core computer vision problem and has many applications, *e.g.*, in autonomous driving [25]. Decades of research efforts have led to impressive performance on challenging benchmarks [4, 11, 17]. Most top-performing methods adopt the energy minimization approach introduced by Horn and Schunck [18]. However, optimizing a complex energy function is usually computationally expensive for real-time applications.

One promising approach is to adopt the fast, scalable, and end-to-end trainable convolutional neural network (CNN) framework [29], which has largely advanced the field of computer vision in recent years. Inspired by the successes of deep learning in high-level vision tasks, Dosovitskiy *et al.* [14] propose two CNN models for optical flow, *i.e.*, FlowNetS and FlowNetC, and introduce a paradigm shift. Their work shows the feasibility of directly estimating optical flow from raw images using a generic U-Net CNN architecture [38]. Although their performances are below the state of the art, FlowNetS and FlowNetC models were the best among their contemporary real-time methods.

Recently, Ilg *et al.* [23] stack several FlowNetC and FlowNetS networks into a large model, called FlowNet2,

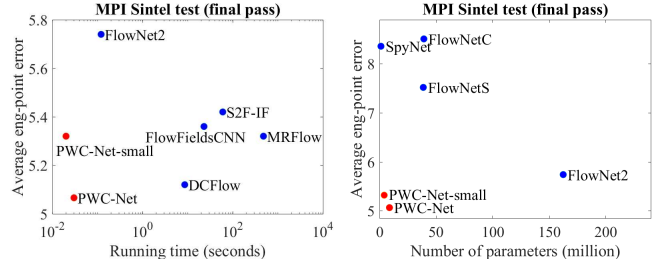


Figure 1. Left: PWC-Net outperforms all published methods on the MPI Sintel final pass benchmark, in terms of both accuracy and running time. Right: PWC-Net reaches the best balance between size and accuracy among existing end-to-end CNN models.

which performs on par with state-of-the-art methods but runs much faster (Fig. 1). However, large models are more prone to the over-fitting problem, and as a result the sub-networks of FlowNet2 have to be trained sequentially. Furthermore, the architecture of FlowNet2 requires a memory footprint of 640MB and is not well-suited for mobile and embedded devices.

SpyNet [36] addresses the model size issue by combining deep learning with two classical optical flow estimation principles. SpyNet uses a spatial pyramid network and warps the second image toward the first one using the initial flow. The motion between the first and warped images is usually small. Thus SpyNet only needs a small CNN network to estimate the motion from these two images. SpyNet performs on par with FlowNetC but below FlowNetS and FlowNet2 (Fig. 1). The results by FlowNet2 and SpyNet show a clear trade-off between model size and accuracy.

In this paper, we ask this question: *is it possible to both increase the accuracy and reduce the size of a CNN model for optical flow?* In principle, the trade-off between model size and accuracy imposes a fundamental limit for general machine learning algorithms. However, we find that combining domain knowledge of optical flow with deep learning can kill two birds with one stone.

SpyNet actually shows the potential of combining classical principles with CNNs. However, we argue that its performance gap with FlowNetS and FlowNet2 is due to the partial use of the classical principles. For example, traditional optical flow methods often pre-process the raw

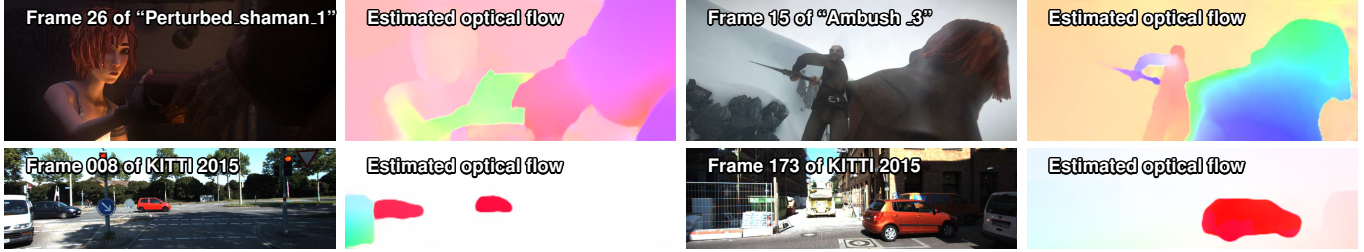


Figure 2. PWC-Net results on Sintel final pass (top) and KITTI 2015 (bottom) test sets. It outperforms all published methods to date.

images to extract features that are invariant to shadows or lighting changes [4]. In the special case of stereo matching, the cost volume is a more discriminative representation of the 1D disparity than raw images [19, 40, 54]. While constructing the full cost volume has been thought to be computationally prohibitive for real-time optical flow estimation [51], we construct a “partial” cost volume by limiting the search range to a few pixels at each pyramid level. The warping layer links different pyramid levels and enables the estimation of large motion.

Our network, called PWC-Net, has been designed to make full use of these simple and well-established principles. It makes significant improvements in terms of model size and accuracy over existing CNN models for optical flow (Figs. 1 and 2). At the time of writing, PWC-Net outperforms all published methods on the challenging Sintel final pass and KITTI 2015 benchmarks. Furthermore, PWC-Net is about 17 times smaller in size and provides 2 times faster inferencing than FlowNet2. It is also easier to train than SpyNet and FlowNet2 and runs at about 35 frames per second (fps) on Sintel resolution ( $1024 \times 436$ ) images.

## 2. Previous Work

**Variational approach.** Horn and Schunck [18] pioneer the variational approach to optical flow by coupling the brightness constancy and spatial smoothness assumptions using an energy function. Black and Anandan [7] introduce a robust framework to deal with outliers, *i.e.*, brightness inconstancy and spatial discontinuities. As it is computationally impractical to perform full search, a coarse-to-fine, warping based approach is often adopted [10]. Brox *et al.* [8] theoretically justify the incremental, warping-based estimation process. Sun *et al.* [42] review the models, optimization, and implementation details for methods derived from Horn and Schunck and propose a non-local prior for optical flow. These methods are effective for small to moderate scale motion, but solving the complex optimization problems is computationally expensive.

One conundrum for the coarse-to-fine, variational approach is small and fast moving objects that disappear at coarse levels. To address this issue, Brox and Malik [9] embed feature matching into the variational framework, which is further improved by follow-up methods [46, 52]. In

particular, the EpicFlow method [37] can effectively interpolate sparse matches to dense optical flow and has been widely used as a post-processing method [1, 3, 13, 20, 51].

Most top-performing methods use CNN models as a component in their system. For example, DCFlow [51], the best-performing published method on MPI Sintel final pass so far, learns features using CNNs, computes the cost volume, and then uses sophisticated post-processing techniques, including EpicFlow, to estimate the optical flow. The second best method, FlowFieldsCNN [3], learns CNN features for sparse matching but still uses EpicFlow to densify the matches. The third one, MRFlow [49] uses a CNN to classify a scene into rigid and non-rigid moving regions and estimates the geometry and camera motion for the rigid region using a plane + parallax formulation. All these methods are neither real-time nor end-to-end trainable.

**Early work on learning optical flow.** Simoncelli and Adelson [41] study the data matching errors for optical flow. Freeman *et al.* [15] learn parameters of an MRF model for image motion using synthetic blob world examples. Roth and Black [39] study the spatial statistics of optical flow based on the fields-of-experts framework using sequences generated from depth maps. Sun *et al.* [43] learn a full model for optical flow, but the learning has been limited to a few training sequences [4]. Li and Huttenlocher [30] use stochastic optimization to tune the parameters for the Black and Anandan method [7], but the number of parameters learned is limited. Wulff and Black [48] learn PCA motion basis of optical flow estimated by GPUFlow [47] on real movies. Their method is fast but tends to produce over-smoothed flow.

**Recent work on learning optical flow.** Inspired by the success of CNNs on high-level vision tasks [28], Dosovitskiy *et al.* [14] construct two CNN networks, FlowNetS and FlowNetC, for estimating optical flow based on the U-Net denoising autoencoder [38]. Pre-trained on a large synthetic “FlyingChairs” dataset, the networks can surprisingly capture the motion of fast moving objects. The raw output of the network, however, tends to contain large errors in smooth background regions and requires variational refinement [9]. Mayer *et al.* [33] apply the FlowNet architecture to disparity and scene flow estimation. Ilg *et al.* [23]

stack several basic FlowNet models into a large one, *i.e.*, FlowNet2, which performs on par with state of the art on the Sintel benchmark. Ranjan and Black [36] develop a highly compact spatial pyramid network, called SpyNet. SpyNet achieves similar performance as the FlowNetC model on the Sintel benchmark, which is good but not state of the art.

Another interesting line of research takes the unsupervised learning approach. Memisevic and Hinton [34] propose the gated restricted Boltzmann machine to learn image transformations in an unsupervised way. Long *et al.* [32] learn CNN models for optical flow by interpolating frames. While inferior to supervised approaches on dataset with labeled training data, existing unsupervised methods can be used to train CNN models in domains without labeled data.

**Cost volume.** Cost volume processing is a standard component for stereo, a special case of optical flow. Recent methods [13, 14, 51] begin to investigate full cost volume processing for optical flow. All these methods build the full cost volume at a single scale, which is both computationally expensive and memory intensive. By contrast, our work shows that constructing partial cost volume at multiple pyramid levels leads to both effective and efficient models.

**Datasets.** Unlike many other vision tasks, it is extremely difficult to obtain ground truth optical flow on real-world sequences. Early work on optical flow mainly relies on synthetic dataset [5], *e.g.*, the famous “Yosemite”. Methods may over-fit to the synthetic data and do not perform well on real data [31]. Baker *et al.* [4] capture real sequences under both ambient and UV lights in controlled lab environment to obtain ground truth, but the approach does not work for outdoor scenes. Liu *et al.* [31] use human annotations to obtain ground truth motion for natural video sequences, but the labeling process is time-consuming.

KITTI and Sintel are currently the most challenging and widely-used benchmarks for optical flow. The KITTI benchmark is targeted for autonomous driving applications and its semi-dense ground truth is collected using LIDAR [17]. The 2012 set consists of static scenes and the 2015 set is extended to dynamic scenes via human annotations [35]. The large motion, severe illumination changes, and occlusions in the 2015 set are challenging to existing methods. The Sintel benchmark [11] is created using the open source graphics movie “Sintel”. It has two passes, clean and final. The final pass contains strong atmospheric effects, motion blur, and camera noise, which cause severe problems to existing methods. The large, nonrigid motion patterns are particularly challenging for end-to-end methods. All published, top-performing methods [3, 49, 51] rely heavily on traditional techniques. By embedding the classical principles into the network architecture, we show that an end-to-end method can outperform all published methods on both the KITTI 2015 and Sintel final pass benchmarks.

**CNN models for dense prediction tasks in vision.** The denoising autoencoder [44] has been commonly used for dense prediction tasks in computer vision, especially with skip connections [38] between the encoder and decoder. Recent work [12, 53] shows that dilated convolution layers can better exploit contextual information and refine details for semantic segmentation. Here we use dilated convolutions in a context network for optical flow and find that it leads to moderate performance improvement. The DenseNet architecture [21, 26], which directly connects each layer to every other layer in a feedforward fashion, has been shown to be more accurate and easier to train than traditional CNN layers in image classification tasks. We test this idea for our task of dense optical flow prediction.

### 3. Approach

Figure 3 summarizes the key components of PWC-Net and compares it side by side with the traditional coarse-to-fine approach [7, 8, 18, 42]. First, it is well-known that raw images do not provide good features to establish correspondence, particularly in the presence of shadows and lighting changes [8, 42]. Thus we replace the fixed image pyramid with learnable *feature pyramids*. Second, we take the *warping* operation from the traditional approach and add it as a layer in our network. Third, as the *cost volume* is a more discriminative representation of the optical flow than raw images, our network has a layer to construct the cost volume, which is then processed by CNN layers to obtain the refined flow. Finally, a common practice by the traditional methods is to post-process the optical flow, such as median filtering [45], weighted median filtering [42], and bilateral filtering [50]. Thus PWC-Net uses a context network to post-process the optical flow. We jointly learn all the parameters, including those of the context network. Compared with energy minimization, the warping, cost volume, and CNN layers are computationally light. Further, the warping and cost volume layers have no learnable parameters and significantly reduce the model size.

Next we will explain the main ideas for each component, including pyramid feature extractor, optical flow estimator, and context networks. Please refer to the appendix for details of the networks.

**Feature pyramid extractor.** Our feature pyramid extractor learns to generate a 7-level pyramid of feature representations for the two input images  $I_1$  and  $I_2$ . At the bottom (zeroth) level, our model convolves the raw images with  $16 \ 3 \times 3$  filters with a stride of 2 to obtain the input features for the first level. At the  $l$ th pyramid level, it downsamples the features from the previous pyramid level  $l - 1$  using layers of convolutional filters to generate the feature representation at the  $l$ th layer,  $c_t^l$ . From the first to the sixth levels, the number of feature channels are respectively 16, 32, 64,

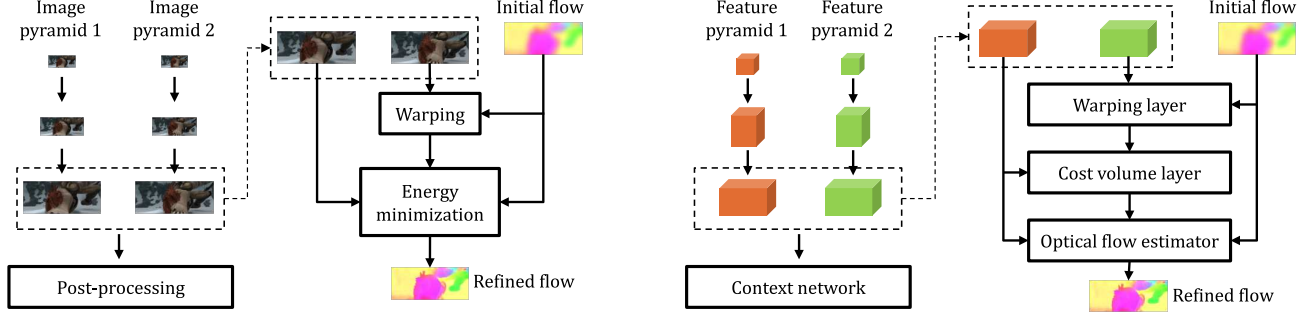


Figure 3. Left: Image pyramid and refinement at one pyramid level by the energy minimization approach [7, 8, 18, 42]. Right: Feature pyramid and refinement at one pyramid level by PWC-Net. PWC-Net *warps* features of the second image using the initial flow, computes the *cost volume*, and process the cost volume using CNNs. Please refer to the text for details about the network.

96, 128, and 196. Features at higher pyramid levels tend to capture global structures, while features at lower levels describe fine details.

**Warping layer.** At the  $l-1$ th level, we warp the feature of the second image,  $c_2^{l-1}$ , toward the first image using the upsampled flow from the  $l$ th level.

$$c_w^{l-1}(\mathbf{x}) = c_2^{l-1}(\mathbf{x} + \uparrow \mathbf{w}^l(\mathbf{x})), \quad (1)$$

where  $\uparrow \mathbf{w}^l$  denotes the upsampled and scaled flow from the  $l$ th level and is zero at the top level. We use the bilinear interpolation method to implement the warping operation and compute the gradients to the input CNN features and flow for backpropagation according to [23, 24]. For non-translational motion, warping can compensate some geometric distortions and place image patches at the right scale.

**Cost volume layer.** At the  $l$ th pyramid level, we obtain the cost volume by computing the correlation [14, 51] using features of the first image,  $c_1^l$ , and warped features of the second image,  $c_w^l$ :

$$cv^l(\mathbf{x}_1, \mathbf{x}_2) = \frac{1}{N} (c_1^l(\mathbf{x}_1))^T c_w^l(\mathbf{x}_2), \quad (2)$$

where  $T$  is the transpose operator and  $N$  is the length of the column vector  $c_1^l(\mathbf{x}_1)$ . For our 7-level pyramid setting, we only need to compute a partial cost volume with a limited range of  $d$  pixels, *i.e.*,  $|\mathbf{x}_1 - \mathbf{x}_2|_\infty \leq d$ . Note that a one-pixel motion at the top level corresponds to 64 ( $2^6$ ) pixels at the full resolution images. Thus we can set  $d$  to be small.

**Optical flow estimator.** To obtain the refined flow  $\mathbf{w}^l$  at the  $l$ th level, the features of the first image, the cost volume, and the upsampled optical flow are fed into a multi-layer CNN, our optical flow estimator. The numbers of feature channels at each convolutional layers are respectively 128, 128, 96, 64, and 32, which are kept fixed at all pyramid levels. Note that the estimators at different levels have their own parameters instead of sharing the same parameters. This process is repeated until we reach the desired

level,  $l_0$ . We set  $l_0$  to be 2 throughout this paper, *i.e.*, our model outputs quarter resolution optical flow and uses bilinear interpolation to obtain the full-resolution optical flow.

The estimator architecture can be enhanced with DenseNet connections [21]. The inputs to every convolutional layer are the output of and the input to its previous layer. DenseNet has more direct connections than traditional layers and leads to significant improvement in image classification. We test this idea for dense flow prediction.

**Context network.** As context is crucial for flow estimation, we employ a context network at the desired pyramid level,  $l_0$ , to effectively enlarge the receptive field size of each output unit. The context network is a feed-forward CNN, takes the estimated flow and features of the second last layer from the estimator, and outputs the refined flow.

The design of the context network is based on dilated convolutions [53]. It consists of 7 convolutional layers. The spatial kernel for each convolutional layer is  $3 \times 3$ . These layers have different dilation constants. A convolutional layer with a dilation constant  $k$  means that an input unit to a filter in the layer are  $k$ -unit apart from the other input units to the filter in the layer, both in vertical and horizontal directions. Convolutional layers with large dilation constants enlarge the receptive field of each output unit without incurring a large computational burden. From bottom to top, the dilation constants are 1, 2, 4, 8, 16, 1, and 1.

**Training loss.** Let  $\Theta$  be the set of all the learnable parameters in our final network, which includes the feature pyramid extractor and the optical flow estimators at different pyramid levels (the warping and cost volume layers have no learnable parameters). Let  $\mathbf{w}_\Theta^l$  denote the flow field at the  $l$ th pyramid level predicted by the network, and  $\mathbf{w}_{GT}^l$  the corresponding supervision signal. We use the same multi-scale training loss proposed in FlowNet [14]:

$$\mathcal{L}(\Theta) = \sum_{l=l_0}^L \alpha_l \sum_{\mathbf{x}} |\mathbf{w}_\Theta^l(\mathbf{x}) - \mathbf{w}_{GT}^l(\mathbf{x})|_2 + \gamma |\Theta|_2, \quad (3)$$



where  $\|\cdot\|_2$  computes the L2 norm of a vector and the second term regularizes parameters of the model. For fine-tuning, we use the following robust training loss

$$\mathcal{L}(\Theta) = \sum_{l=l_0}^L \alpha_l \sum_{\mathbf{x}} (|\mathbf{w}_{\Theta}^l(\mathbf{x}) - \mathbf{w}_{\text{GT}}^l(\mathbf{x})| + \epsilon)^q + \gamma \|\Theta\|_2 \quad (4)$$

where  $\|\cdot\|_1$  denotes the L1 norm,  $q < 1$  gives less penalty to outliers, and  $\epsilon$  is a small constant.

## 4. Experimental Results

**Implementation details.** The weights in the training loss (3) are set to be  $\alpha_6 = 0.32$ ,  $\alpha_5 = 0.08$ ,  $\alpha_4 = 0.02$ ,  $\alpha_3 = 0.01$ , and  $\alpha_2 = 0.005$ . This setting gives higher weights to loss terms at the second and third pyramid levels, if we take the number of pixels at each level into account. We scale the ground truth flow by 20 and downsample it to obtain the supervision signals at different levels. Note that we do not further scale the supervision signal at each level, the same as [14]. As a result, we need to scale the upsampled flow at each pyramid level for the warping layer. For example, at the second level, we scale the upsampled flow from the third level by a factor of 5 ( $= 20/4$ ) before warping features of the second image. The trade-off weight  $\gamma$  is set to be 0.0004. For the cost volume, we set the search range to be 4 pixels at each level.

We first train the models using the “FlyingChairs” dataset in Caffe [27] using the  $S_{long}$  learning rate schedule introduced in [23], *i.e.*, starting from 0.0001 and reducing the learning rate by half at 0.4M, 0.6M, 0.8M, and 1M iterations. The data augmentation scheme is the same as that in [23]. We crop  $448 \times 384$  patches during data augmentation and use a batch size of 8. Next we fine-tune the models on the “FlyingThings” dataset using the  $S_{fine}$  schedule. The cropped image size is  $768 \times 384$  and the batch size is 4. Finally, we fine-tune the models using the Sintel and KITTI training set and will explain the details below.

### 4.1. Main Results

**MPI Sintel.** When fine-tuning on Sintel, we crop  $768 \times 384$  image patches during data augmentation and use a batch size of 4. We also use the robust loss function in Eq. (4) with  $\epsilon = 0.01$  and  $q = 0.4$ . We test two schemes of fine-tuning. The first one, PWC-Net-ft, uses the clean and final passes of the Sintel training data throughout the fine-tuning process. The second one, PWC-Net-ft-final, uses only the final pass for the second half of fine-tuning. We test the second scheme because the DCFlow method learns the features using only the final pass of the training data. Thus we are interested in the performance of PWC-Net when the final pass of the training data is given more weight.

At the time of writing, PWC-Net has lower average end-point error (EPE) than all published methods on the

final pass of the MPI-Sintel benchmark (Table 1). It is the first time that an end-to-end method outperforms well-engineered and highly fine-tuned traditional methods on this benchmark. Further, PWC-Net is the fastest among all the top-performing methods. We can further reduce the running time by dropping the DenseNet connections. The resulting PWC-Net-small model is about 5% less accurate but 40% faster than PWC-Net.

PWC-Net is not as accurate as traditional approaches on the clean pass. Many traditional methods use image edges to refine motion boundaries, because the two are perfectly aligned in the clean pass. However, image edges in the final pass have been smoothed and corrupted by motion blur, atmospheric changes, and noise. Thus, the final pass is more realistic and challenging for traditional approaches. The results on the final and clean sets suggest that PWC-Net may be better suited for real images, where the image edges are often corrupted.

Compared with FlowNet2, PWC-Net has higher errors on the training set but lower errors on the test set, suggesting that PWC-Net may have a more appropriate capacity for this task. Table 2 summarizes the errors in different regions. PWC-Net performs relatively better in regions with large motion and away from the motion boundaries, probably because it has been trained using only data with large displacements. Figure 4 shows the visual results of different variants of PWC-Net on the training and test sets of MPI Sintel. PWC-Net can recover sharp motion boundaries but may fail on small and rapidly moving objects, such as the left arm in “Market\_5”.

Table 1. Average EPE results on MPI Sintel set. “-ft” means fine-tuning on the MPI Sintel *training* set and the numbers in the parenthesis are results on the data the methods have been fine-tuned on. ft-final gives more weight to the final pass during fine-tuning.

Methods	Training		Test		Time (s)
	Clean	Final	Clean	Final	
PatchBatch [16]	-	-	5.79	6.78	50.0
EpicFlow [37]	-	-	4.12	6.29	15.0
CPM-flow [20]	-	-	3.56	5.96	4.30
FullFlow [13]	-	3.60	2.71	5.90	240
FlowFields [2]	-	-	3.75	5.81	28.0
MRFlow [49]	1.83	3.59	<b>2.53</b>	5.38	480
FlowFieldsCNN [3]	-	-	3.78	5.36	23.0
DCFlow [51]	-	-	3.54	5.12	8.60
SpyNet-ft [36]	(3.17)	(4.32)	6.64	8.36	0.16
FlowNet2.0 [23]	2.02	3.14	3.96	6.02	0.12
FlowNet2.0-ft [23]	<b>(1.45)</b>	<b>(2.01)</b>	4.16	5.74	0.12
PWC-Net-small	2.83	4.08	-	-	<b>0.02</b>
PWC-Net-small-ft	(2.27)	(2.45)	5.05	5.32	<b>0.02</b>
PWC-Net	2.55	3.93	-	-	0.03
PWC-Net-ft	(1.70)	(2.21)	3.86	5.13	0.03
PWC-Net-ft-final	(2.02)	(2.08)	4.39	<b>5.04</b>	0.03

**KITTI.** When fine-tuning on KITTI, we crop  $896 \times 320$  image patches during data augmentation and use a batch size of 4. The large patches can capture the large motion



Figure 4. Results on Sintel *training* and *test* sets. Context network, DenseNet connections, and fine-tuning all improve the results.

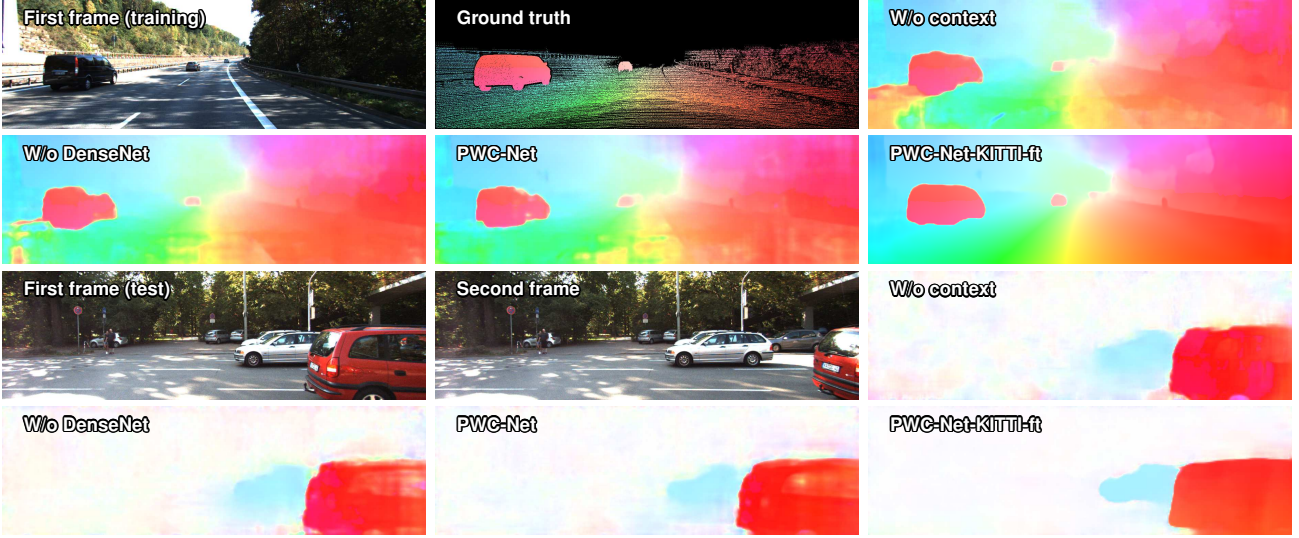


Figure 5. Results on KITTI 2015 *training* and *test* sets. Fine-tuning fixes large regions of errors and recovers sharp motion boundaries.

Table 2. Detailed results on the Sintel benchmark for different regions, velocities ( $s$ ), and distances from motion boundaries ( $d$ ).

Final	matched	unmatched	$d_{0-10}$	$d_{10-60}$	$d_{60-140}$	$s_{0-10}$	$s_{10-40}$	$s_{40+}$
PWC-Net	<b>2.44</b>	<b>27.08</b>	<b>4.68</b>	<b>2.08</b>	<b>1.52</b>	<b>0.90</b>	<b>2.99</b>	<b>31.28</b>
FlowNet2	2.75	30.11	4.82	2.56	1.74	0.96	3.23	35.54
SpyNet	4.51	39.69	6.69	4.37	3.29	1.40	5.53	49.71
clean								
PWC-Net	<b>1.45</b>	<b>23.47</b>	3.83	<b>1.31</b>	<b>0.56</b>	0.70	2.19	<b>23.56</b>
FlowNet2	1.56	25.40	<b>3.27</b>	1.46	0.86	<b>0.60</b>	<b>1.89</b>	27.35
SpyNet	3.01	36.19	5.50	3.12	1.72	0.83	3.34	43.44

in the KITTI dataset. Since the ground truth is semi-dense, we upsample the predicted flow at the quarter resolution and directly compare the upscaled flow with the scaled ground truth at the full resolution. We exclude the invalid pixels in computing the loss function.

At the time of writing, PWC-Net outperforms all published two-frame optical flow methods on the 2015 set, as shown in Table 3. It has the lowest percentage of flow outliers (Fl-all) in both all and non-occluded pixels (Table 4). In terms of speed, PWC-Net is the fastest among all top-

Table 3. Results on the KITTI dataset. “-ft” means fine-tuning on the KITTI *training* set and the numbers in the parenthesis are results on the data the methods have been fine-tuned on.

Methods	KITTI 2012			KITTI 2015		
	AEPE <i>train</i>	AEPE <i>test</i>	Fl-Noc <i>test</i>	AEPE <i>train</i>	Fl-all <i>train</i>	Fl-all <i>test</i>
EpicFlow [37]	-	3.8	7.88%	-	-	26.29 %
FullFlow [13]	-	-	-	-	-	23.37 %
CPM-flow [20]	-	3.2	5.79%	-	-	22.40 %
PatchBatch [16]	-	3.3	5.29%	-	-	21.07%
FlowFields [2]	-	-	-	-	-	19.80%
MRFlow [49]	-	-	-	-	14.09 %	12.19 %
DCFlow [51]	-	-	-	-	15.09 %	14.83 %
SDF [1]	-	2.3	<b>3.80%</b>	-	-	11.01 %
MirrorFlow [22]	-	2.6	4.38%	-	9.93%	10.29%
SpyNet-ft [36]	(4.13)	4.7	12.31%	-	-	35.07%
FlowNet2 [23]	4.09	-	-	10.06	30.37%	-
FlowNet2-ft [23]	<b>(1.28)</b>	1.8	4.82%	(2.30)	<b>(8.61%)</b>	10.41 %
PWC-Net	4.14	-	-	10.35	33.67%	-
PWC-Net-ft	(1.45)	<b>1.7</b>	4.22%	<b>(2.16)</b>	(9.80%)	<b>9.60%</b>

Table 4. Detailed Results on the KITTI 2015 benchmark for the top three optical flow and two scene flow methods (below).

Methods	Non-occluded pixels			All pixels		
	Fl-bg	Fl-fg	Fl-all	Fl-bg	Fl-fg	Fl-all
MirrorFlow [22]	6.24%	12.95%	7.46%	<b>8.93%</b>	17.07%	10.29%
FlowNet2 [23]	7.24%	<b>5.60%</b>	6.94%	10.75%	<b>8.75%</b>	10.41%
PWC-Net	<b>6.14%</b>	5.98%	<b>6.12%</b>	9.66%	9.31%	<b>9.60%</b>
OSF [35]	<b>4.21%</b>	15.49%	6.26%	5.62%	18.92%	7.83%
ISF [6]	<b>4.21%</b>	<b>6.83%</b>	<b>4.69%</b>	<b>5.40%</b>	<b>10.29%</b>	<b>6.22%</b>

performing methods. PWC-Net has the second lowest percentage of outliers in non-occluded regions (Fl-noc) on the 2012 set, only inferior to SDF that assumes rigidity constraint for the background. Although the rigidity assumption works well on the static scenes in the 2012 set, PWC-Net outperforms SDF in the 2015 set which mainly consists of dynamic scenes and is more challenging.

As shown in Table 4, FlowNet2 and PWC-Net have the most accurate results in the foreground regions, both outperforming the best published scene flow method, ISF [6]. Scene flow methods, however, have much lower errors in the static background region. The results suggest that combining advances in optical flow and scene flow could lead to more accurate results.

The visual results in Fig. 5 qualitatively demonstrate the benefits of using the context network, DenseNet connections, and fine-tuning respectively. In particular, fine-tuning fixes large regions of errors in the test set, demonstrating the benefit of learning when the training and test data have similar statistics.

## 4.2. Ablation Experiments

To analyze PWC-Net, we run a number of ablations. Table 5 summarizes the key results and the appendix provides more results.

**Feature pyramid extractor.** PWC-Net uses a two-layer CNN to extract features at each pyramid level. Table 5a

summarizes the results of two variants that use one layer ( $\downarrow$ ) and three layers ( $\uparrow$ ) respectively. Larger-capacity feature pyramid extractor leads to consistently better results on both the training and validation datasets.

**Optical flow estimator.** PWC-Net uses a five-layer CNN in the optical flow estimator at each level. Table 5b shows the results by two variants that use four layer ( $\downarrow$ ) and seven layers ( $\uparrow$ ) respectively. Larger-capacity optical flow estimator leads to better performance. However, we observe in our experiments that a deeper optical flow estimator might get stuck in a poor local minimum, which can be detected early by checking the validation errors after a few thousand iterations and fixed by a complete new run.

Removing the context network results in larger errors on both the training and validation sets (Table 5c). Removing the DenseNet connections results in higher training error but lower validation errors when the model is trained on “FlyingChairs”. However, after the model is fine-tuned on “FlyingThings3D”, DenseNet leads to lower errors.

We further test a residual version of the optical flow estimator, which estimates a flow increment and adds it to the initial flow for the refined flow. As shown in Table 5f, this residual version slightly improves the performance.

**Cost volume.** Next we test the search range to compute the cost volume, shown in Table 5d. Larger range leads to lower training error. However, all three settings have similar performance on Sintel, because a range of 2 at every level can already deal with motion up to 200 pixels at the input resolution. A larger range has lower EPE on KITTI, likely because the images from the KITTI dataset have larger displacements than those from Sintel. A smaller range, however, seems to force the network to ignore pixels with extremely large motion and focus more on small-motion pixels, thereby achieving lower F-all scores.

**Warping.** Warping allows for estimating a small optical flow (increment) at each pyramid level to deal with large optical flow. Removing the warping layers results in a significant loss in accuracy (Table 5e). Without the warping layer, PWC-Net still produces reasonable results, because the default search range of 4 to compute the cost volume is large enough to capture the motion of most sequences at the low-resolution pyramid levels.

**Dataset scheduling.** We also train PWC-Net using different dataset scheduling schemes, as shown in Table 6. Sequentially training on “FlyingChairs”, “FlyingThings3D”, and Sintel gradually improves the performance, consistent with the observations in [23]. Directly training using the test data leads to good “over-fitting” results, but the trained model does not perform as well on other datasets.



	Chairs	Sintel Clean	Sintel Final	KITTI 2012		KITTI 2015	
				AEPE	Fl-all	AEPE	Fl-all
Full model	2.00	3.33	4.59	5.14	28.67%	13.20	41.79%
Feature $\uparrow$	<b>1.92</b>	<b>3.03</b>	<b>4.17</b>	<b>4.57</b>	<b>26.73%</b>	<b>11.64</b>	<b>39.80%</b>
Feature $\downarrow$	2.18	3.36	4.56	5.75	30.79%	14.05	44.92%

(a) Larger-capacity **feature pyramid extractor** has better performance.

	Trained on FlyingChairs			Fine-tuned on FlyingThings		
	Chairs	Clean	Final	Chairs	Clean	Final
Full model	<b>2.00</b>	3.33	4.59	<b>2.34</b>	<b>2.60</b>	<b>3.95</b>
No Densenet	2.06	<b>3.09</b>	<b>4.37</b>	2.48	2.83	4.08
No Context	2.23	3.47	4.74	2.55	2.75	4.13

(c) **Context network** consistently helps; **DenseNet** helps after fine-tuning.

	Chairs	Sintel Clean	Sintel Final	KITTI 2012		KITTI 2015	
				AEPE	Fl-all	AEPE	Fl-all
Full model	<b>2.00</b>	<b>3.33</b>	<b>4.59</b>	<b>5.14</b>	<b>28.67%</b>	<b>13.20</b>	<b>41.79%</b>
No warping	2.17	3.79	5.30	5.80	32.73%	13.74	44.87%

(e) **Warping layer** is a critical component for the performance.

	Chairs	Sintel Clean	Sintel Final	KITTI 2012		KITTI 2015	
				AEPE	Fl-all	AEPE	Fl-all
Full model	2.00	3.33	4.59	5.14	28.67%	13.20	41.79%
Estimator $\uparrow$	<b>1.92</b>	<b>3.09</b>	<b>4.50</b>	<b>4.64</b>	<b>25.34%</b>	<b>12.25</b>	<b>39.18%</b>
Estimator $\downarrow$	2.01	3.37	4.58	4.82	26.35%	12.83	40.53%

(b) Larger-capacity **optical flow estimator** has better performance.

Max. Disp.	Chairs	Sintel Clean	Sintel Final	KITTI 2012		KITTI 2015	
				AEPE	Fl-all	AEPE	Fl-all
Full model	2.00	3.33	4.59	5.14	28.67%	13.20	41.79%
2	2.09	<b>3.30</b>	<b>4.50</b>	5.26	<b>25.99%</b>	13.67	<b>38.99%</b>
6	<b>1.97</b>	3.31	4.60	<b>4.96</b>	27.05%	<b>12.97</b>	40.94%

(d) **Cost volume**. PWC-Net can handle large motion with small search range.

	Chairs	Sintel Clean	Sintel Final	KITTI 2012		KITTI 2015	
				AEPE	Fl-all	AEPE	Fl-all
Full model	2.00	3.33	4.59	5.14	28.67%	13.20	41.79%
Residual	<b>1.96</b>	<b>3.14</b>	<b>4.43</b>	<b>4.87</b>	<b>27.74%</b>	<b>12.58</b>	<b>41.16%</b>

(f) **Residual connections** in the optical flow estimator are helpful.

Table 5. **Ablation experiments**. Unless explicitly stated, the models have been trained on the “FlyingChairs” dataset.

Table 6. **Training dataset schedule** leads to better local minima.

(.) indicates results on the dataset the method has been trained on.

Data	Chairs AEPE	Sintel (AEPE) Clean	Final	KITTI 2012 AEPE	KITTI 2012 Fl-all	KITTI 2015 AEPE	KITTI 2015 Fl-all
Chairs	<b>(2.00)</b>	3.33	4.59	5.14	28.67%	13.20	41.79%
Chairs-Things	2.30	2.55	3.93	4.14	21.38%	10.35	33.67%
Chairs-Things-Sintel	2.56	<b>(1.70)</b>	<b>(2.21)</b>	<b>2.94</b>	<b>12.70%</b>	<b>8.15</b>	<b>24.35%</b>
Sintel	3.69	(1.86)	(2.31)	3.68	16.65%	10.52	30.49%

**Model size and running time.** Table 7 summarizes the model size for different CNN models. PWC-Net has about 17 times fewer parameters than FlowNet2. PWC-Net-small halves the parameters by dropping DenseNet connections, and is more suitable for memory-limited applications.

The timings have been obtained on the same desktop using an NVIDIA Pascal TitanX GPU. For more precise timing, we exclude the reading and writing time when benchmarking the forward and backward inference time. PWC-Net is about 2 times faster in forward inference and at least 3 times faster in training than FlowNet2.

Table 7. **Model size and running time.** PWC-Net-small drops Densenet connections. For training, the lower bound of 14 days for FlowNet2 is obtained by 6(FlowNetC) + 2 $\times$ 4 (FlowNetS).

Methods	FlowNetS	FlowNetC	FlowNet2	SpyNet	PWC-Net	PWC-Net-small
#parameters (M)	38.67	39.17	162.49	1.2	8.75	4.08
Parameter Ratio	23.80%	24.11%	100%	0.74%	5.38%	2.51%
Memory (MB)	154.5	156.4	638.5	9.7	41.1	22.9
Memory Ratio	24.20%	24.49%	100%	1.52%	6.44%	3.59%
Training (days)	4	6	>14	-	4.8	4.1
Forward (ms)	11.40	21.69	84.80	-	28.56	20.76
Backward (ms)	16.71	48.67	78.96	-	44.37	28.44

**Discussions.** Both PWC-Net and SpyNet have been inspired by classical principles for flow and stereo but have significant differences. SpyNet uses an image pyramid while ours builds a learnable feature pyramids. SpyNet feeds the CNNs with two input images, while PWC-Net

feeds the cost volume. As the cost volume is a more discriminative representation of the search space for optical flow, the learning task for the CNN becomes easier. In terms of performance, PWC-Net outperforms SpyNet by a significant margin. In addition, SpyNet has to be trained in a sequential fashion, while PWC-Net can be trained end-to-end from scratch.

FlowNet2 [23] achieves impressive performance by stacking several basic models into a large-capacity model. While the more compact PWC-Net achieves similar or better performance, it may still be interesting to use PWC-Net as a building block to design larger networks.

## 5. Conclusions

We have developed a compact but effective CNN model for optical flow using three simple and well-established principles: pyramidal processing, warping, and the use of a cost volume. Using domain knowledge not only reduces the model size but also increases the accuracy. PWC-Net is about 17 times smaller in size, 2 times faster in inference, and easier to train than FlowNet2. It outperforms all published methods to date on the MPI Sintel final pass and KITTI 2015 benchmarks, running at about 35 fps on Sintel resolution (1024 $\times$ 436) images. Given the compactness, efficiency, and effectiveness of PWC-Net, we expect it to be a useful component of many video processing systems.

This work shows the benefits of combining deep learning with domain knowledge. To enable comparison and further innovations, we will make our model publicly available.

## References

- [1] M. Bai, W. Luo, K. Kundu, and R. Urtasun. Exploiting semantic information and deep matching for optical flow. In



- European Conference on Computer Vision (ECCV)*, 2016. [2](#), [7](#), [17](#)
- [2] C. Bailer, B. Taetz, and D. Stricker. Flow fields: Dense correspondence fields for highly accurate large displacement optical flow estimation. In *IEEE International Conference on Computer Vision (ICCV)*, 2015. [5](#), [7](#)
  - [3] C. Bailer, K. Varanasi, and D. Stricker. Cnn-based patch matching for optical flow with thresholded hinge embedding loss. In *IEEE Conference on Computer Vision and Pattern Recognition (CVPR)*, 2017. [2](#), [3](#), [5](#)
  - [4] S. Baker, D. Scharstein, J. P. Lewis, S. Roth, M. J. Black, and R. Szeliski. A database and evaluation methodology for optical flow. *International Journal of Computer Vision (IJCV)*, 2011. [1](#), [2](#), [3](#)
  - [5] J. Barron, D. Fleet, and S. Beauchemin. Performance of optical flow techniques. *International Journal of Computer Vision (IJCV)*, 1994. [3](#)
  - [6] A. Behl, O. H. Jafari, S. K. Mustikovela, H. A. Alhaija, C. Rother, and A. Geiger. Bounding boxes, segmentations and object coordinates: How important is recognition for 3d scene flow estimation in autonomous driving scenarios? In *ICCV*, 2017. [7](#)
  - [7] M. J. Black and P. Anandan. The robust estimation of multiple motions: Parametric and piecewise-smooth flow fields. *Computer Vision and Image Understanding (CVIU)*, 1996. [2](#), [3](#), [4](#)
  - [8] T. Brox, A. Bruhn, N. Papenberger, and J. Weickert. High accuracy optical flow estimation based on a theory for warping. In *European Conference on Computer Vision (ECCV)*, 2004. [2](#), [3](#), [4](#)
  - [9] T. Brox and J. Malik. Large displacement optical flow: Descriptor matching in variational motion estimation. *TPAMI*, 2011. [2](#)
  - [10] A. Bruhn, J. Weickert, and C. Schnörr. Lucas/Kanade meets Horn/Schunck: combining local and global optic flow methods. *International Journal of Computer Vision (IJCV)*, 2005. [2](#)
  - [11] D. J. Butler, J. Wulff, G. B. Stanley, and M. J. Black. A naturalistic open source movie for optical flow evaluation. In *European Conference on Computer Vision (ECCV)*, 2012. [1](#), [3](#)
  - [12] L. C. Chen, G. Papandreou, I. Kokkinos, K. Murphy, and A. L. Yuille. Deeplab: Semantic image segmentation with deep convolutional nets, atrous convolution, and fully connected crfs. *TPAMI*, 2017. [3](#)
  - [13] Q. Chen and V. Koltun. Full flow: Optical flow estimation by global optimization over regular grids. In *IEEE Conference on Computer Vision and Pattern Recognition (CVPR)*, 2016. [2](#), [3](#), [5](#), [7](#)
  - [14] A. Dosovitskiy, P. Fischery, E. Ilg, C. Hazirbas, V. Golkov, P. van der Smagt, D. Cremers, T. Brox, et al. FlowNet: Learning optical flow with convolutional networks. In *IEEE International Conference on Computer Vision (ICCV)*, 2015. [1](#), [2](#), [3](#), [4](#), [5](#)
  - [15] W. T. Freeman, E. C. Pasztor, and O. T. Carmichael. Learning low-level vision. *International Journal of Computer Vision (IJCV)*, 2000. [2](#)
  - [16] D. Gadot and L. Wolf. Patchbatch: a batch augmented loss for optical flow. In *IEEE Conference on Computer Vision and Pattern Recognition (CVPR)*, 2016. [5](#), [7](#)
  - [17] A. Geiger, P. Lenz, and R. Urtasun. Are we ready for autonomous driving? The KITTI vision benchmark suite. In *IEEE Conference on Computer Vision and Pattern Recognition (CVPR)*, 2012. [1](#), [3](#)
  - [18] B. Horn and B. Schunck. Determining optical flow. *Artificial Intelligence*, 1981. [1](#), [2](#), [3](#), [4](#)
  - [19] A. Hosni, C. Rhemann, M. Bleyer, C. Rother, and M. Gelautz. Fast cost-volume filtering for visual correspondence and beyond. *TPAMI*, 2013. [2](#)
  - [20] Y. Hu, R. Song, and Y. Li. Efficient coarse-to-fine patch-match for large displacement optical flow. In *IEEE Conference on Computer Vision and Pattern Recognition (CVPR)*, 2016. [2](#), [5](#), [7](#)
  - [21] G. Huang, Z. Liu, K. Q. Weinberger, and L. van der Maaten. Densely connected convolutional networks. In *IEEE Conference on Computer Vision and Pattern Recognition (CVPR)*, 2017. [3](#), [4](#)
  - [22] J. Hur and S. Roth. Mirrorflow: Exploiting symmetries in joint optical flow and occlusion estimation. In *IEEE International Conference on Computer Vision (ICCV)*, Oct 2017. [7](#)
  - [23] E. Ilg, N. Mayer, T. Saikia, M. Keuper, A. Dosovitskiy, and T. Brox. FlowNet 2.0: Evolution of optical flow estimation with deep networks. In *IEEE Conference on Computer Vision and Pattern Recognition (CVPR)*, 2017. [1](#), [2](#), [4](#), [5](#), [7](#), [8](#)
  - [24] M. Jaderberg, K. Simonyan, A. Zisserman, et al. Spatial transformer networks. In *Advances in Neural Information Processing Systems (NIPS)*, 2015. [4](#)
  - [25] J. Janai, F. Güney, A. Behl, and A. Geiger. Computer vision for autonomous vehicles: Problems, datasets and state-of-the-art. *arXiv preprint arXiv:1704.05519*, 2017. [1](#)
  - [26] S. Jégou, M. Drozdal, D. Vazquez, A. Romero, and Y. Bengio. The one hundred layers tiramisu: Fully convolutional densenets for semantic segmentation. In *IEEE Conference on Computer Vision and Pattern Recognition (CVPR) Workshop*, 2017. [3](#)
  - [27] Y. Jia, E. Shelhamer, J. Donahue, S. Karayev, J. Long, R. Girshick, S. Guadarrama, and T. Darrell. Caffe: Convolutional architecture for fast feature embedding. In *ACM Multimedia*, 2014. [5](#)
  - [28] A. Krizhevsky, I. Sutskever, and G. E. Hinton. Imagenet classification with deep convolutional neural networks. In *Advances in Neural Information Processing Systems (NIPS)*, 2012. [2](#)
  - [29] Y. LeCun, B. Boser, J. S. Denker, D. Henderson, R. E. Howard, W. Hubbard, and L. D. Jackel. Backpropagation applied to handwritten zip code recognition. *Neural computation*, 1989. [1](#)
  - [30] Y. Li and D. P. Huttenlocher. Learning for optical flow using stochastic optimization. In *European Conference on Computer Vision (ECCV)*, 2008. [2](#)
  - [31] C. Liu, W. T. Freeman, E. H. Adelson, and Y. Weiss. Human-assisted motion annotation. In *IEEE Conference on Computer Vision and Pattern Recognition (CVPR)*, 2008. [3](#)

- [32] G. Long, L. Kneip, J. M. Alvarez, H. Li, X. Zhang, and Q. Yu. Learning image matching by simply watching video. In *European Conference on Computer Vision (ECCV)*, 2016. 3
- [33] N. Mayer, E. Ilg, P. Häusser, P. Fischer, D. Cremers, A. Dosovitskiy, and T. Brox. A large dataset to train convolutional networks for disparity, optical flow, and scene flow estimation. In *CVPR*, 2016. 2
- [34] R. Memisevic and G. Hinton. Unsupervised learning of image transformations. In *IEEE Conference on Computer Vision and Pattern Recognition (CVPR)*, 2007. 3
- [35] M. Menze and A. Geiger. Object scene flow for autonomous vehicles. In *CVPR*, 2015. 3, 7
- [36] A. Ranjan and M. J. Black. Optical flow estimation using a spatial pyramid network. In *IEEE Conference on Computer Vision and Pattern Recognition (CVPR)*, 2017. 1, 3, 5, 7
- [37] J. Revaud, P. Weinzaepfel, Z. Harchaoui, and C. Schmid. EpicFlow: Edge-Preserving Interpolation of Correspondences for Optical Flow. In *CVPR*, 2015. 2, 5, 7
- [38] O. Ronneberger, P. Fischer, and T. Brox. U-net: Convolutional networks for biomedical image segmentation. In *MICCAI*, 2015. 1, 2, 3
- [39] S. Roth and M. J. Black. On the spatial statistics of optical flow. *International Journal of Computer Vision (IJCV)*, 2007. 2
- [40] D. Scharstein and R. Szeliski. A taxonomy and evaluation of dense two-frame stereo correspondence algorithms. *International Journal of Computer Vision (IJCV)*, 2002. 2
- [41] E. P. Simoncelli, E. H. Adelson, and D. J. Heeger. Probability distributions of optical flow. In *IEEE Conference on Computer Vision and Pattern Recognition (CVPR)*, 1991. 2
- [42] D. Sun, S. Roth, and M. J. Black. A quantitative analysis of current practices in optical flow estimation and the principles behind them. *International Journal of Computer Vision (IJCV)*, 2014. 2, 3, 4
- [43] D. Sun, S. Roth, J. P. Lewis, and M. J. Black. Learning optical flow. In *European Conference on Computer Vision (ECCV)*, 2008. 2
- [44] P. Vincent, H. Larochelle, Y. Bengio, and P.-A. Manzagol. Extracting and composing robust features with denoising autoencoders. In *International Conference on Machine Learning (ICML)*, 2008. 3
- [45] A. Wedel, T. Pock, C. Zach, D. Cremers, and H. Bischof. An improved algorithm for TV-L1 optical flow. In *Dagstuhl Motion Workshop*, 2008. 3
- [46] P. Weinzaepfel, J. Revaud, Z. Harchaoui, and C. Schmid. DeepFlow: Large displacement optical flow with deep matching. In *IEEE International Conference on Computer Vision (ICCV)*, 2013. 2
- [47] M. Werlberger, W. Trobin, T. Pock, A. Wedel, D. Cremers, and H. Bischof. Anisotropic Huber-L1 optical flow. In *British Machine Vision Conference (BMVC)*, 2009. 2
- [48] J. Wulff and M. J. Black. Efficient sparse-to-dense optical flow estimation using a learned basis and layers. In *CVPR*, pages 120–130, 2015. 2
- [49] J. Wulff, L. Sevilla-Lara, and M. J. Black. Optical flow in mostly rigid scenes. In *IEEE Conference on Computer Vision and Pattern Recognition (CVPR)*, 2017. 2, 3, 5, 7
- [50] J. Xiao, H. Cheng, H. Sawhney, C. Rao, and M. Isnardi. Bilateral filtering-based optical flow estimation with occlusion detection. In *European Conference on Computer Vision (ECCV)*, 2006. 3
- [51] J. Xu, R. Ranftl, and V. Koltun. Accurate optical flow via direct cost volume processing. In *IEEE Conference on Computer Vision and Pattern Recognition (CVPR)*, 2017. 2, 3, 4, 5, 7
- [52] L. Xu, J. Jia, and Y. Matsushita. Motion detail preserving optical flow estimation. *TPAMI*, 2012. 2
- [53] F. Yu and V. Koltun. Multi-scale context aggregation by dilated convolutions. In *International Conference on Learning Representations (ICLR)*, 2016. 3, 4
- [54] J. Zbontar and Y. LeCun. Stereo matching by training a convolutional neural network to compare image patches. *Journal of Machine Learning Research (JMLR)*, 2016. 2

In this appendix, Section A provides more ablation and visual comparison results. Section B summarizes the details of our network. Section C shows the screen shot of the MPI Sintel final pass, KITTI 2012, and KITTI 2015 public table taken on Nov. 15th, 2017. Section D shows the learned features at the first level of the feature pyramid extractor.

## A. More Ablation and Visual Results

Figure 6 shows the enlarged images of the Figure 1 in the main manuscript. PWC-Net outperforms all published methods on the MPI Sintel final pass benchmark, in terms of both accuracy and running time. It also reaches the best balance between size and accuracy among existing end-to-end CNN models.

Table 8 shows more ablation results, in particular, the full results for models trained on “FlyingChairs” (Table 8a) and then fine-tuned on “FlyingThings3D” (Table 8b). To further test the dilated convolutions, we replace the dilated convolutions of the context network with plain convolutions. Using plain convolutions has worse performance on Chairs and Sintel, and is slightly better on KITTI. We also have independent runs of the same PWC-Net that only differ in the random initialization. As shown in Table 8d, the two independent runs leads to models that have close performance, although not exactly the same.

Figures 7 and 8 provide more visual results by PWC-Net on the MPI Sintel final pass and KITTI 2015 test sets. PWC-Net can recover sharp motion boundaries in the presence of large motion, severe occlusions, and strong shadow and atmospheric effects. However, PWC-Net tends to produce errors on objects with thin structure that rarely occurs in the training set, such as the wheels of the bicycle in the third row of Figure 8.

## B. Network Details

Figure 9 shows the architecture for the 7-level feature pyramid extractor network used in our experiment. Note that the bottom level consists of the original input images. Figure 10 shows the optical flow estimator network at pyramid level 2. The optical flow estimator networks at other levels have the same structure except the top level, which does not have the upsampled optical flow and directly computes cost volume using features of the first and second images. Figure 11 shows the context network at pyramid level 2.

## C. Screen Shots of Sintel and KITTI Public Table

Figures 12-14 respectively show the screen shots of the MPI Sintel final pass, KITTI 2015, and KITTI 2012 public tables as of November 15th, 2017. Among all optical flow

methods, PWC-Net is ranked 1st on both MPI Sintel final and KITTI 2015, and 2nd on KITTI 2012. Note that the SDF method that has lower percentage of outliers in non-occluded regions than PWC-Net on KITTI 2015 uses rigidity constraint for the background, which is well-suited to the static scenes in KITTI 2012.

## D. Learned Features

Figure 15 shows the learned filters for the first convolution layer by PWCD-DC and the feature responses to an input image. These filters tend to focus on regions of different properties in the input image. After training on “FlyingChairs”, fine-tuning on “FlyingThings3D” and Sintel does not change these filters much.



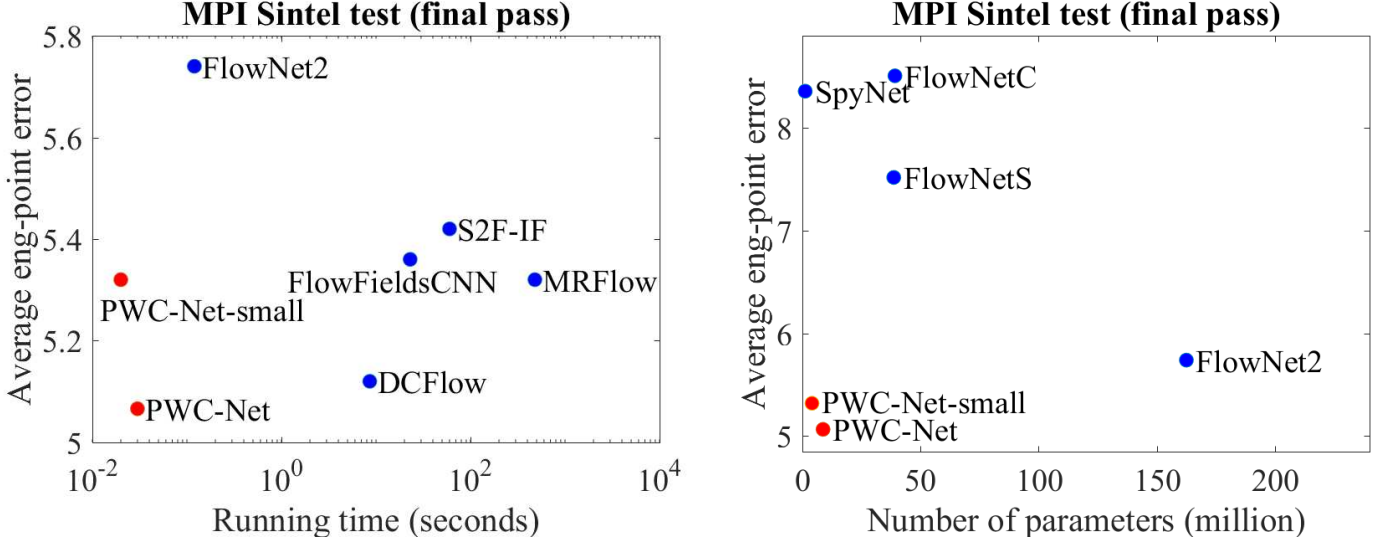


Figure 6. Left: PWC-Net outperforms all published methods on the MPI Sintel final pass benchmark, in terms of both accuracy and running time. Right: PWC-Net reaches the best balance between size and accuracy among existing end-to-end CNN models.

	Chairs	Sintel Clean	Sintel Final	KITTI 2012 AEPE	KITTI 2012 Fl-all	KITTI 2015 AEPE	KITTI 2015 Fl-all
Full model	<b>2.00</b>	3.33	4.59	5.14	28.67%	13.20	41.79%
No context	2.06	<b>3.09</b>	<b>4.37</b>	<b>4.77</b>	<b>25.35%</b>	<b>12.03</b>	<b>39.21%</b>
No DenseNet	2.23	3.47	4.74	5.63	28.53%	14.02	40.33%
Neither	2.22	3.15	4.49	5.46	28.02%	13.14	40.03%

(a) Trained on “FlyingChairs”.

	Chairs	Sintel Clean	Sintel Final	KITTI 2012 AEPE	KITTI 2012 Fl-all	KITTI 2015 AEPE	KITTI 2015 Fl-all
Full model	<b>2.30</b>	<b>2.55</b>	<b>3.93</b>	<b>4.14</b>	<b>21.38%</b>	<b>10.35</b>	<b>33.67%</b>
No context	2.48	2.82	4.09	4.39	21.91%	10.82	34.44%
No DenseNet	2.54	2.72	4.09	4.91	24.04%	11.52	34.79%
Neither	2.65	2.83	4.24	4.89	24.52%	12.01	35.73%

(b) Fine-tuned on “FlyingThings3D” after “FlyingChairs”.

	Chairs	Sintel Clean	Sintel Final	KITTI 2012 AEPE	KITTI 2012 Fl-all	KITTI 2015 AEPE	KITTI 2015 Fl-all
Dilated conv	<b>2.00</b>	<b>3.33</b>	<b>4.59</b>	<b>5.14</b>	28.67%	13.20	41.79%
Plain conv	2.03	3.39	4.85	5.29	<b>25.86%</b>	<b>13.17</b>	<b>38.67%</b>

(c) Dilated vs plain convolutions for the context network.

	Chairs	Sintel Clean	Sintel Final	KITTI 2012 AEPE	KITTI 2012 Fl-all	KITTI 2015 AEPE	KITTI 2015 Fl-all
Run 1	2.00	3.33	<b>4.59</b>	5.14	28.67%	13.20	41.79%
Run 2	<b>2.00</b>	<b>3.33</b>	4.65	<b>4.81</b>	<b>27.12%</b>	<b>13.10</b>	<b>40.84%</b>

(d) Two independent runs result in slightly different models.

Table 8. More ablation experiments. Unless explicitly stated, the models have been trained on the “FlyingChairs” dataset.



Figure 7. More PWC-Net results on Sintel final pass dataset.



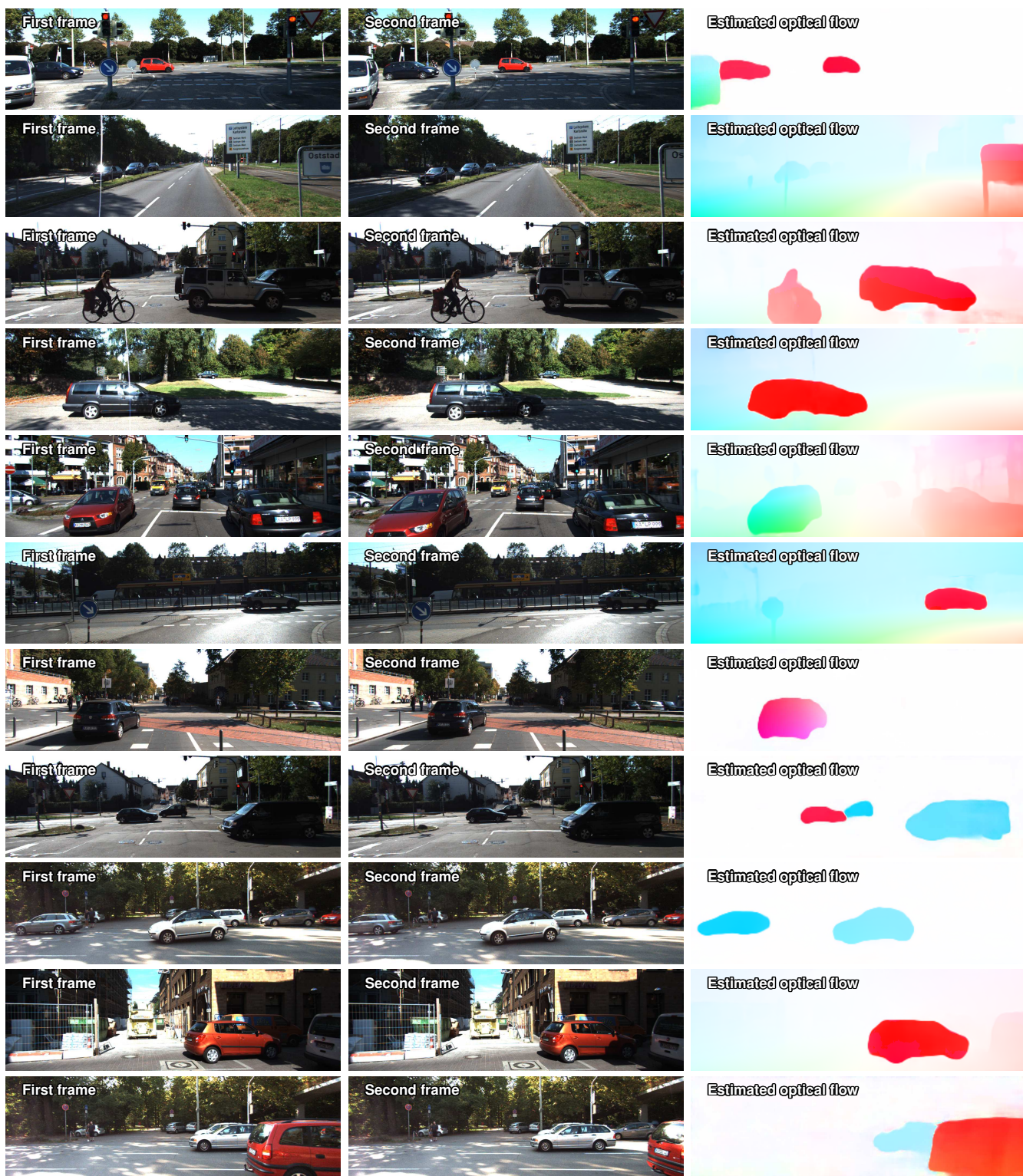


Figure 8. More PWC-Net results on KITTI 2015 test set. PWC-Net can recover sharp motion boundaries despite large motion, strong shadows, and severe occlusions. Thin structures, such as the bicycle, is challenging to PWC-Net, probably the training set does not have enough training samples of bicycles.



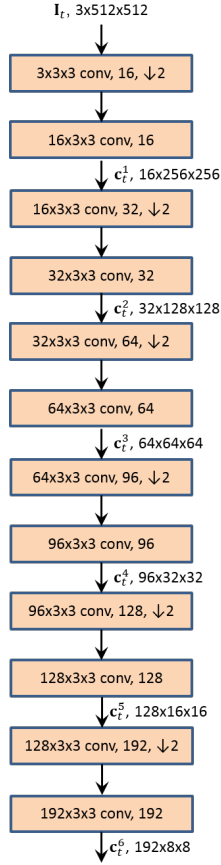


Figure 9. The feature pyramid extractor network. The first image ( $t = 1$ ) and the second image ( $t = 2$ ) are encoded using the same Siamese network. Each convolution is followed by a leaky ReLU unit. The convolutional layer and the  $\times 2$  downsampling layer at each level is implemented using a single convolutional layer with a stride of 2.  $c_t^l$  denotes extracted features of image  $t$  at level  $l$ ;

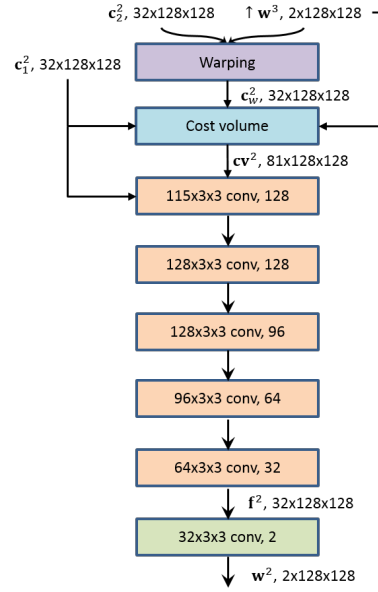


Figure 10. The optical flow estimator network at pyramid level 2. Each convolutional layer is followed by a leaky ReLU unit except the last (light green) one that outputs the optical flow.

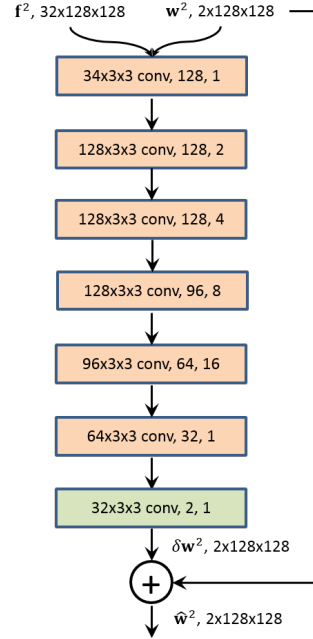


Figure 11. The context network at pyramid level 2. Each convolutional layer is followed by a leaky ReLU unit except the last (light green) one that outputs the optical flow. The last number in each convolutional layer denotes the dilation constant.

Final Clean

	EPE all	EPE matched	EPE unmatched	d0-10	d10-60	d60-140	s0-10	s10-40	s40+	
GroundTruth <sup>[1]</sup>	0.000	0.000	0.000	0.000	0.000	0.000	0.000	0.000	0.000	<a href="#">Visualize Results</a>
<b>PWC-Net <sup>[2]</sup></b>	5.042	2.445	26.221	4.636	2.087	1.475	0.799	2.986	31.070	<a href="#">Visualize Results</a>
DCFlow <sup>[3]</sup>	5.119	2.283	28.228	4.665	2.108	1.440	1.052	3.434	29.351	<a href="#">Visualize Results</a>
FlowFieldsCNN <sup>[4]</sup>	5.363	2.303	30.313	4.718	2.020	1.399	1.032	3.065	32.422	<a href="#">Visualize Results</a>
MR-Flow <sup>[5]</sup>	5.376	2.818	26.235	5.109	2.395	1.755	0.908	3.443	32.221	<a href="#">Visualize Results</a>
FTFlow <sup>[6]</sup>	5.390	2.268	30.841	4.513	1.964	1.366	1.046	3.322	31.936	<a href="#">Visualize Results</a>
S2F-IF <sup>[7]</sup>	5.417	2.549	28.795	4.745	2.198	1.712	1.157	3.468	31.262	<a href="#">Visualize Results</a>
InterpNet_ff <sup>[8]</sup>	5.535	2.372	31.296	4.720	2.018	1.532	1.064	3.496	32.633	<a href="#">Visualize Results</a>
PGM-C <sup>[9]</sup>	5.591	2.672	29.389	4.975	2.340	1.791	1.057	3.421	33.339	<a href="#">Visualize Results</a>
RicFlow <sup>[10]</sup>	5.620	2.765	28.907	5.146	2.366	1.679	1.088	3.364	33.573	<a href="#">Visualize Results</a>
InterpNet_cpm <sup>[11]</sup>	5.627	2.594	30.344	4.975	2.213	1.640	1.042	3.575	33.321	<a href="#">Visualize Results</a>

Figure 12. Screen shot of the MPI Sintel final pass public table. PWC-Net has the lowest average end-point error (EPE) among all evaluated methods as of November 15th, 2017.

Evaluation ground truth All pixels Evaluation area All pixels

	Method	Setting	Code	FI-bg	FI-fg	FI-all	Density	Runtime	Environment	Compare
1	<a href="#">PSPO</a>			4.35 %	15.21 %	6.15 %	100.00 %	5 min	1 core @ 2.5 Ghz (Matlab + C/C++)	<input type="checkbox"/>
2	<a href="#">ISF</a>			5.40 %	10.29 %	6.22 %	100.00 %	10 min	1 core @ 3 Ghz (C/C++)	<input type="checkbox"/>
A. Behl, O. Jafari, S. Mustikovela, H. Alhajja, C. Rother and A. Geiger: <a href="#">Bounding Boxes, Segmentations and Object Coordinates: How Important is Recognition for 3D Scene Flow Estimation in Autonomous Driving Scenarios?</a> . International Conference on Computer Vision (ICCV) 2017.										
3	<a href="#">PRSM</a>		<a href="#">code</a>	5.33 %	13.40 %	6.68 %	100.00 %	300 s	1 core @ 2.5 Ghz (C/C++)	<input type="checkbox"/>
C. Vogel, K. Schindler and S. Roth: <a href="#">3D Scene Flow Estimation with a Piecewise Rigid Scene Model</a> . ijcv 2015.										
4	<a href="#">OSF+TC</a>			5.76 %	13.31 %	7.02 %	100.00 %	50 min	1 core @ 2.5 Ghz (C/C++)	<input type="checkbox"/>
M. Neoral and J. Šochman: <a href="#">Object Scene Flow with Temporal Consistency</a> . 22nd Computer Vision Winter Workshop (CVWW) 2017.										
5	<a href="#">SSF</a>			5.63 %	14.71 %	7.14 %	100.00 %	5 min	1 core @ 2.5 Ghz (Matlab + C/C++)	<input type="checkbox"/>
Z. Ren, D. Sun, J. Kautz and E. Sudderth: <a href="#">Cascaded Scene Flow Prediction using Semantic Segmentation</a> . International Conference on 3D Vision (3DV) 2017.										
6	<a href="#">SOSF</a>			5.42 %	17.24 %	7.39 %	100.00 %	55 min	1 core @ 2.5 Ghz (Matlab + C/C++)	<input type="checkbox"/>
7	<a href="#">OSF</a>		<a href="#">code</a>	5.62 %	18.92 %	7.83 %	100.00 %	50 min	1 core @ 2.5 Ghz (C/C++)	<input type="checkbox"/>
M. Menze and A. Geiger: <a href="#">Object Scene Flow for Autonomous Vehicles</a> . Conference on Computer Vision and Pattern Recognition (CVPR) 2015.										
8	<b>PWC-Net</b>			9.66 %	9.31 %	9.60 %	100.00 %	0.03 s	NVIDIA Pascal Titan X	<input type="checkbox"/>
9	<a href="#">MirrorFlow</a>			8.93 %	17.07 %	10.29 %	100.00 %	11 min	4 core @ 2.2 Ghz (C/C++)	<input type="checkbox"/>
J. Hur and S. Roth: <a href="#">MirrorFlow: Exploiting Symmetries in Joint Optical Flow and Occlusion Estimation</a> . ICCV 2017.										
10	<a href="#">FlowNet2</a>			10.75 %	8.75 %	10.41 %	100.00 %	0.12 s	GPU Nvidia GeForce GTX 1080	<input type="checkbox"/>
11	<a href="#">SDF</a>			8.61 %	23.01 %	11.01 %	100.00 %	TBA	1 core @ 2.5 Ghz (C/C++)	<input type="checkbox"/>
M. Bai*, W. Luo*, K. Kundu and R. Urtasun: <a href="#">Exploiting Semantic Information and Deep Matching for Optical Flow</a> . ECCV 2016.										
12	<a href="#">UnFlow</a>			10.15 %	15.93 %	11.11 %	100.00 %	0.12 s	GPU @ 1.5 Ghz (Python + C/C++)	<input type="checkbox"/>
S. Meister, J. Hur and S. Roth: <a href="#">UnFlow: Unsupervised Learning of Optical Flow with a Bidirectional Census Loss</a> . AAAI 2018.										
13	<a href="#">FSF+MS</a>			8.48 %	25.43 %	11.30 %	100.00 %	2.7 s	4 cores @ 3.5 Ghz (C/C++)	<input type="checkbox"/>
T. Tanial, S. Sinha and Y. Sato: <a href="#">Fast Multi-frame Stereo Scene Flow with Motion Segmentation</a> . IEEE Conference on Computer Vision and Pattern Recognition (CVPR) 2017.										
14	<a href="#">CNNF+PMBP</a>			10.08 %	18.56 %	11.49 %	100.00 %	45 min	1 cores @ 3.5 Ghz (C/C++)	<input type="checkbox"/>
15	<a href="#">MR-Flow</a>		<a href="#">code</a>	10.13 %	22.51 %	12.19 %	100.00 %	8 min	1 core @ 2.5 Ghz (Python + C/C++)	<input type="checkbox"/>
J. Wulff, L. Sevilla-Lara and M. Black: <a href="#">Optical Flow in Mostly Rigid Scenes</a> . IEEE Conf. on Computer Vision and Pattern Recognition (CVPR) 2017.										

Figure 13. Screen shot of the KITTI 2015 public table. PWC-Net has the lowest percentage of error among all optical flow methods, only inferior to scene flow methods that use additional stereo input information.

Error threshold 3 pixels ▾ Evaluation area All pixels ▾

	Method	Setting	Code	Out-Noc	Out-All	Avg-Noc	Avg-All	Density	Runtime	Environment	Compare
1	<a href="#">PRSM</a>		<a href="#">code</a>	2.46 %	4.23 %	0.7 px	1.0 px	100.00 %	300 s	1 core @ 2.5 Ghz (Matlab + C/C++)	<input type="checkbox"/>
C. Vogel, K. Schindler and S. Roth: <a href="#">3D Scene Flow Estimation with a Piecewise Rigid Scene Model</a> . <i>ijcv</i> 2015.											
2	<a href="#">VC-SF</a>			2.72 %	4.84 %	0.8 px	1.3 px	100.00 %	300 s	1 core @ 2.5 Ghz (Matlab + C/C++)	<input type="checkbox"/>
C. Vogel, S. Roth and K. Schindler: <a href="#">View-Consistent 3D Scene Flow Estimation over Multiple Frames</a> . <i>Proceedings of European Conference on Computer Vision. Lecture Notes in, Computer Science</i> 2014.											
3	<a href="#">SPS-StFI</a>			2.82 %	5.61 %	0.8 px	1.3 px	100.00 %	35 s	1 core @ 3.5 Ghz (C/C++)	<input type="checkbox"/>
K. Yamaguchi, D. McAllester and R. Urtasun: <a href="#">Efficient Joint Segmentation, Occlusion Labeling, Stereo and Flow Estimation</a> . <i>ECCV</i> 2014.											
4	<a href="#">SPS-FI</a>			3.38 %	10.06 %	0.9 px	2.9 px	100.00 %	11 s	1 core @ 3.5 Ghz (C/C++)	<input type="checkbox"/>
K. Yamaguchi, D. McAllester and R. Urtasun: <a href="#">Efficient Joint Segmentation, Occlusion Labeling, Stereo and Flow Estimation</a> . <i>ECCV</i> 2014.											
5	<a href="#">OSF</a>		<a href="#">code</a>	3.47 %	6.34 %	1.0 px	1.5 px	100.00 %	50 min	1 core @ 3.0 Ghz (Matlab + C/C++)	<input type="checkbox"/>
M. Menze and A. Geiger: <a href="#">Object Scene Flow for Autonomous Vehicles</a> . <i>Conference on Computer Vision and Pattern Recognition (CVPR)</i> 2015.											
6	<a href="#">PR-Sf+E</a>			3.57 %	7.07 %	0.9 px	1.6 px	100.00 %	200 s	4 cores @ 3.0 Ghz (Matlab + C/C++)	<input type="checkbox"/>
C. Vogel, K. Schindler and S. Roth: <a href="#">Piecewise Rigid Scene Flow</a> . <i>International Conference on Computer Vision (ICCV)</i> 2013.											
7	<a href="#">PCBP-Flow</a>			3.64 %	8.28 %	0.9 px	2.2 px	100.00 %	3 min	4 cores @ 2.5 Ghz (Matlab + C/C++)	<input type="checkbox"/>
K. Yamaguchi, D. McAllester and R. Urtasun: <a href="#">Robust Monocular Epipolar Flow Estimation</a> . <i>CVPR</i> 2013.											
8	<a href="#">PR-SceneFlow</a>			3.76 %	7.39 %	1.2 px	2.8 px	100.00 %	150 sec	4 core @ 3.0 Ghz (Matlab + C/C++)	<input type="checkbox"/>
C. Vogel, K. Schindler and S. Roth: <a href="#">Piecewise Rigid Scene Flow</a> . <i>International Conference on Computer Vision (ICCV)</i> 2013.											
9	<a href="#">SDF</a>			3.80 %	7.69 %	1.0 px	2.3 px	100.00 %	TBA s	1 core @ 2.5 Ghz (C/C++)	<input type="checkbox"/>
M. Bai*, W. Luo*, K. Kundu and R. Urtasun: <a href="#">Exploiting Semantic Information and Deep Matching for Optical Flow</a> . <i>ECCV</i> 2016.											
10	<a href="#">MotionSLIC</a>			3.91 %	10.56 %	0.9 px	2.7 px	100.00 %	11 s	1 core @ 3.0 Ghz (C/C++)	<input type="checkbox"/>
K. Yamaguchi, D. McAllester and R. Urtasun: <a href="#">Robust Monocular Epipolar Flow Estimation</a> . <i>CVPR</i> 2013.											
11	<a href="#">PWC-Net</a>			4.22 %	8.10 %	0.9 px	1.7 px	100.00 %	0.03 s	NVIDIA Pascal Titan X	<input type="checkbox"/>
12	<a href="#">TBR</a>			4.24 %	7.50 %	0.9 px	1.5 px	100.00 %	1750 s	4 cores @ 2.5 Ghz (Matlab + C/C++)	<input type="checkbox"/>
13	<a href="#">UnFlow</a>			4.28 %	8.42 %	0.9 px	1.7 px	100.00 %	0.12 s	GPU @ 1.5 Ghz (Python + C/C++)	<input type="checkbox"/>
S. Meister, J. Hur and S. Roth: <a href="#">UnFlow: Unsupervised Learning of Optical Flow with a Bidirectional Census Loss</a> . <i>AAAI</i> 2018.											
14	<a href="#">MirrorFlow</a>			4.38 %	8.20 %	1.2 px	2.6 px	100.00 %	11 min	4 core @ 2.2 Ghz (C/C++)	<input type="checkbox"/>
J. Hur and S. Roth: <a href="#">MirrorFlow: Exploiting Symmetries in Joint Optical Flow and Occlusion Estimation</a> . <i>ICCV</i> 2017.											

Figure 14. Screen shot of the KITTI 2012 public table. SDF [9] is the only optical flow method that has lower percentage of outliers in non-occluded regions (FI-Noc score) than PWC-Net. However, SDF assumes rigidity for the background, which is well-suited for the static scenes in the 2012 set.



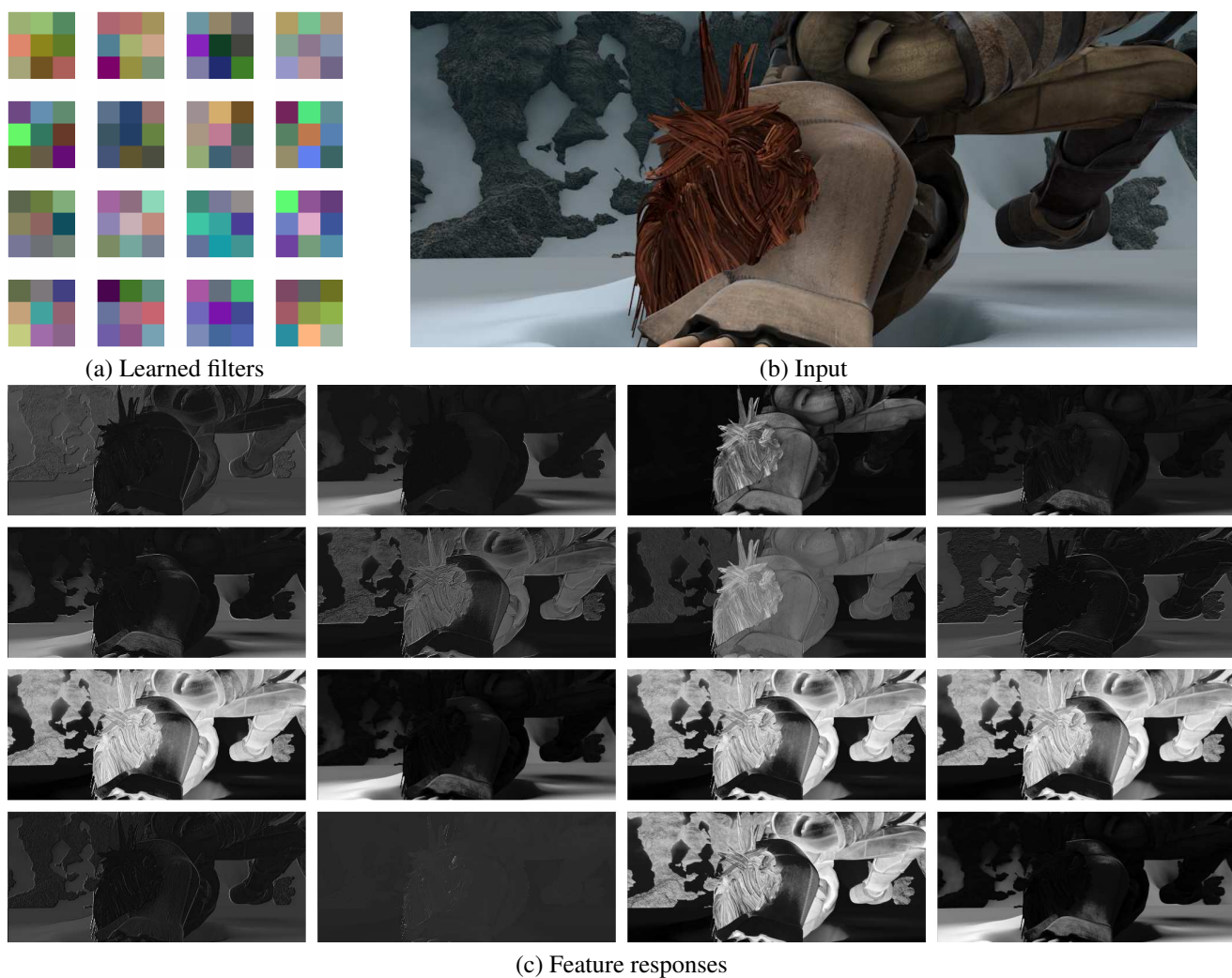


Figure 15. Learned filters in the first convolutional layer of PWC-Net and the filter responses to an input image.